



Published in final edited form as:

J Immunol. 2016 June 1; 196(11): 4632–4640. doi:10.4049/jimmunol.1502218.

Myeloid-restricted AMPK α 1 promotes host immunity and protects against IL12/23p40-dependent lung injury during hookworm infection

Wildaliz Nieves*, Li-Yin Hung*, Taylor K. Oniskey*, Louis Boon†, Marc Foretz‡,§,¶, Benoit Viollet‡,§,¶, and De'Broski R. Herbert*,¹

*Department of Medicine, Division of Experimental Medicine, University of California, San Francisco, California, United States of America

†EPIRUS Biopharmaceuticals, Netherlands BV

‡Institut National de la Santé et de la Recherche Médicale U1016, Institut Cochin, Paris, France

§Centre National de la Recherche Scientifique, Unités Mixtes de Recherche 8104, Paris, France

¶Université Paris Descartes, Sorbonne Paris cité, Paris, France

Abstract

How the metabolic demand of parasitism affects immune-mediated resistance is poorly understood. Immunity against parasitic helminthes requires M2 cells and interleukin-13 (IL-13), secreted by CD4⁺ T_H2 and group 2 innate lymphoid cells (ILC2), but whether certain metabolic enzymes control disease outcome has not been addressed. This study demonstrates that AMP-activated protein kinase (AMPK), a key driver of cellular energy, regulates Type 2 immunity and restricts lung injury following hookworm infection. Mice with a selective deficiency in the AMPK catalytic α 1 subunit in alveolar macrophages and conventional DC (cDC) produced less IL-13, and CCL17, and had impaired expansion of ILC2 in damaged lung tissue compared to wild-type controls. Defective Type 2 responses were marked by increased intestinal worm burdens, exacerbated lung injury, and increased production of IL-12/23p40, which, when neutralized, restored IL-13 production and improved lung recovery. Taken together, these data indicate that defective AMPK activity in myeloid cells negatively impacts Type 2 responses through increased IL-12/23p40 production. These data support an emerging concept that myeloid cells and ILC2 can coordinately regulate tissue damage at mucosal sites through mechanisms dependent upon metabolic enzyme function.

Introduction

The AMPK complex ($\alpha\beta\gamma$); comprised of an α catalytic subunit with serine/threonine kinase activity, β glycogen-binding domain and γ adenylate-binding region, coordinates glucose metabolism with fatty acid oxidation to regulate energy availability (1, 2). AMPK may regulate genes in muscle and adipose tissue by phosphorylation of specific transcription

¹Corresponding Author: De'Broski R. Herbert Ph.D., ; Email: debroski.herbert@ucsf.edu, Office: 415-206-8177 Fax: 415-206-8091.

factors involved in glucose metabolism, mitochondrial biogenesis, or fatty acid oxidation (3). However, the roles served by AMPK in the myeloid lineage, particularly during pathogen-specific immune responses, are not well understood.

Mononuclear phagocytes (macrophages and DC) can serve influential roles in the development of Type 2 immunity against parasitic helminthes (4). Humans infected with hookworms present with symptoms of dysregulated metabolic homeostasis including anemia, fatigue, malnutrition, and impaired T cell responses (5), any of which could be due to altered function(s) of myeloid phagocytes. Infection-associated immunosuppression due to worms is closely associated with IL-4/IL-13-driven M2c polarization characterized by increased production of Ym-1 (chitinase-like protein 3) and resistin-like molecule (RELM)- α (6). AMPK promotes an M1 to M2 conversion, as demonstrated in mouse models of muscle tissue damage, multiple sclerosis, and LPS-induced inflammation (7–9), but whether myeloid-intrinsic AMPK controls the outcome of Type 2 responses during infection has not been addressed.

Similar to many helminth species, hookworms cause transient, alveolar lung damage (distal lung space) within the host (10). *N. brasiliensis* (*N.b.*), a rodent hookworm, causes hemorrhagic lung injury within the first 3 dpi, which causes the release of cytokines like IL-33 to initiate Type 2 immunity. IL-33-driven host resistance relies upon IL-13 secreted by CD4⁺ T_H2 and ILC2 lymphoid cells for RELM- β -dependent killing (11–13). Whilst macrophage depletion exacerbates T_H17-associated inflammation and lung damage (14), the question of whether metabolic control of M2 cells promotes lung tissue repair has not been answered. Herein, we demonstrate that AMPK α 1 is required for CD11c-expressing myeloid cells to promote ILC2 expansion, Type 2 immune resistance, and lung tissue repair during *N.b.* infection. AMPK deficiency in macrophages and cDC impaired host protection, marked by increased numbers of adult worms and fecal egg numbers, reduced IL-13 cytokine secretion, and reduced ILC2 expansion in an IL-12/23p40-dependent manner. Thus, our data reveal a previously unrecognized role for myeloid-restricted AMPK as an important driver of Type 2 responses involving ILC2 expansion that precedes lung tissue repair and expulsion of GI nematodes from the intestinal tract.

Materials and Methods

Ethics Statement

Animal experiments were conducted in accordance to University of California at San Francisco Institutional Animal Care and Use Committee protocol AN088478-03 (PI-DRH) and the National Public Health Service (PHS Assurance # A3400-01). These procedures approved under the University Administrative Policy # 100-17 Research and Instruction Using Animal Subjects.

Animals and Parasites

CD11c^{Cre} (Jackson Laboratories, #008068) were bred with previously described AMPK^{flox/flox} mice on a C57BL/6 background (7). Either CD11c^{Cre} or AMPK α 1^{flox/flox} littermates were used for wild-type (WT) controls. Age-matched mice between 6-12 weeks

old were used and housed at the SFGH vivarium. *N.b.* life cycle and techniques for subcutaneous inoculation with 750 *N.b.* third-stage larvae (L3), quantitation of worm burdens and fecal eggs has been described previously (11).

ELISA

A pAMPK α [T172]-specific ELISA Kit (Invitrogen) was used to quantify pAMPK levels in lung tissue homogenates following the manufacturer's instruction. pAMPK levels were normalized to the total protein content of sample as determined by a BCA Assay (Pierce). Cytokine ELISAs IL-13 (eBiosciences) and Ym-1 (R&D) were carried out per manufacturer protocol.

Antibodies and flow cytometry

To determine the frequency of pAMPK α ⁺ cells, whole lungs were processed as previously described (12). To obtain a single suspension of whole splenocytes, tissue was passed through a 100 μ m sieve prior to lysis of red blood cells. Once a single cell suspension was achieved, cells were stained with the cell viability dye ef506 (eBioscience) prior to myeloid cell surface staining using CD11c (N418, Biolegend), Siglec-F (3D6.112, Biolegend), MHC-II (M5-114.15.2, eBiosciences), CD103 (2E7, eBiosciences), and CD11b (M170, Tonbo Biosciences) or T cell staining CD62L (MEL-14, Tonbo Biosciences), CD44 (IM7, Biolegend) CD4 (GK1.5 eBiosciences), and CD8a (5H10, Invitrogen). Cells were stained intracellularly per the manufacturer protocol using rabbit anti-mouse pAMPK α [Y365] mAb (Abcam) or isotype control rabbit anti-mouse IgG primary antibody and anti-rabbit-APC secondary antibody.

To determine the frequency of IL-13-producing CD4⁺ T cells, mice were administered 0.5 mg/ml of Brefeldin A (Sigma) i.p. 5-6 hr prior to processing of whole splenocytes to obtain a single cell suspension. Cells were stained with the cell viability dye ef506 (eBioscience) prior to T cell surface staining as described above including B220 (RA36B2, eBiosciences), F4/80 (BM8, eBiosciences), CD11b (M1/70, eBiosciences), and CD11c (N418, eBiosciences) lineage negative markers. Following fixation and permeabilization using the BD Cytofix/CytoPerm kit (BD Biosciences), ICS of IL-13 (I3A, eBiosciences) was performed overnight at 4°C

To determine the percent and total lung ILC2, whole lungs were processed to obtain a single cell suspension and live cells were quantified using a Guava Cell Counter (EMD-Millipore). A lineage negative cell isolation kit was used (Miltenyi Biotec) (anti-CD4, CD11c, B220, NK1.1) to enrich for ILC2 by magnetic bead-based purification (negative selection) followed by enumeration of the live cells in the flow through. This was used as the total lung cell number for calculation of ILC2 percentage. Cells were incubated with Fc-block (clone 2.4G2) prior to surface staining with a lineage-specific antibody cocktail: anti-B220 (RA3-6B2), CD4 (GK1.5), CD8a (53-6.7), CD11b (M1/70), CD11c (N418), Gr1 (RB6-8C5), and CD49b (DX5). Lineage negative cells were further analyzed using fluorescently-conjugated mAb specific for anti-Thy1.2 (30-H12), CD45 (30-F11), IL-7R β (A7R34), and GATA3 (TWAJ) to identify the ILC2 population. An LSR-II (BD Biosciences)

flow cytometer was used to acquire cells. Data was analyzed using FlowJo (Tree Star) software.

Neutralization of IL-12/23p40 was achieved by administering 1 mg of anti-IL-12/23p40 mAb (C17.8) or isotype control (GL117) intra-peritoneally (i.p.) every 48 h over 9 days.

Histology

Perfused formalin-fixed paraffin-embedded whole lung tissue cross-sections were stained with H&E. Composite “stitched” images (5x magnification) were generated using LAS V4.3 imaging acquisition software to visualize an entire lobe.

Pulse oximetry

Blood oxygen levels (% SpO₂) were measured using MouseOx® Plus with a small CollarClip (STARR Life Sciences Corp.). Mouse hair on the sensor site was removed one day before oximetry per the manufacturer recommendations. On the day of measuring, mice were anesthetized and one minute of oximetry was recorded and analyzed. Results were obtained as percentage of oxygen saturation (% SpO₂), which was a readout from MouseOx® Plus. The mean ± SE % SpO₂ was obtained per time-point for each mouse and the change in % SpO₂ was calculated by subtracting from baseline values.

Real-time PCR analysis

Total RNA was harvested from tissues using RNeasy Mini kit (QIAGEN) following the manufacturer's protocol. 500 ng of total RNA was reverse-transcribed using Superscript II (Invitrogen) following the manufacturer's protocol. Diluted cDNA samples were added to SsoAdvanced SYBR® Green Supermix (Bio-Rad) and RT-PCR reactions were run on CFX96 RT-PCR detection system (Bio-Rad). Primer sequences are listed on Table 1 of Supplemental Materials. Gene expression is normalized to *Gapdh* and data were presented as mean ± SEM from the replicates.

Statistics

The statistical significance of differences between two or more groups was determined by an unpaired Student's t-test, the Mann-Whitney test, One-way ANOVA, or a 2-way ANOVA. P-values greater than 0.05 were considered significant. All analysis was performed using GraphPad Prism 5.0 software.

Results

Myeloid cell-specific AMPK α 1 activation exacerbates hookworm-mediated lung injury

Using pulse oximetry, we established a non-invasive method for tracking the change in percent blood oxygenation (% SpO₂) over the course of hookworm infection. WT mice infected with 750 *N.b.* larvae had a 30% reduction in % SpO₂ by 3 days post-infection (dpi), but % SpO₂ levels rebounded to baseline within 9-12 dpi (Figure 1A). To investigate whether parasitized tissue underwent any change in AMPK activity, experiments were designed to compare whole lung AMPK activity between naïve and *N.b.*-infected WT mice. Results from a phospho-AMPK (pAMPK) α -specific ELISA revealed a 2-fold increase in

AMPK activation within whole lung tissue of WT mice at 3 dpi (Figure 1B). Increased AMPK activation corresponded to the nadir in % SpO₂ assessed via pulse oximetry. Next, to determine whether myeloid cells were a functionally important source of AMPK, mice with a conditional defect of AMPK α 1 in alveolar macrophages and conventional dendritic cells (CD11cAMPK) were generated following an intercross between CD11c^{Cre} and AMPK α 1^{flox/flox} mouse strains and compared to wild-type controls (CD11c^{Cre}).

To confirm CD11c^{Cre} specificity, intracellular flow cytometry was used to identify the AMPK α -deleted cell populations. As expected, staining with pAMPK α -specific mAb in naïve alveolar macrophages revealed a 3-fold reduction in MFI compared to WT (Figure 2 A, B). Similarly, following *N.b.* infection, alveolar macrophages, but not eosinophils showed a 2-3 fold reduction in pAMPK α MFI when isolated from CD11cAMPK compared to WT (Figure 2 C-F). The CD11cAMPK strain also deleted AMPK α protein in MHC-II^{Hi} CD11b⁺ DCs, but not CD103⁺ DCs or interstitial macrophages (Figure 2 G-J). Next, we quantified AMPK activation within whole lung tissue of CD11cAMPK mice following *N.b.* infection. Curiously, the infection induced increase in AMPK activity was unabated in the lung tissues of CD11cAMPK strain (Figure 2K), which was most likely due to the compensatory increase in pAMPK α MFI levels within CD4⁺ or CD8⁺ T lymphocytes; a feature noted both at baseline and during infection (Figure 2 L-R). CD11cAMPK mice displayed no defect in ILC2 expression of AMPK α 1 (data not shown). We postulated that while overall tissue AMPK levels were not reduced in CD11cAMPK mice, selective AMPK deficiency in the myeloid compartment could limit the nature of the immune response against worm infection and potentially impact the rate of lung recovery following *N.b.* infection.

Consistent with our hypothesis, while there were no baseline defects in % SpO₂ levels among naïve mice of control or AMPK mutants (Figure 3A), we found that CD11c-restricted AMPK α 1 deletion had a striking impact upon the rebound of % SpO₂ levels following hookworm-induced lung injury (Figure 3B). The % SpO₂ nadir caused by *N.b.* was significantly greater in CD11cAMPK mice at 3 dpi compared to WT and also the late phase rebound in lung function at day 8 was significantly impaired in the former compared to the latter (Figure 3B). Comparative analysis of lung histological tissue sections from naïve vs. *N.b.* inoculated mice at 9 dpi revealed numerous denuded tissue areas with large distended alveoli, whereas WT lung tissues had normal compact alveolar structure that was consistent with resolution of tissue damage (Figure 3C-G). Myeloid restricted AMPK also changed the inflammatory response, as determined by differential cell staining of bronchoalveolar lavage (BAL) fluid recovered from WT and CD11cAMPK at 9 dpi. Data show that while both strains had the similar numbers of macrophages, there was a reduction in eosinophils and an increase in neutrophils within infected CD11cAMPK mice compared to their WT counterparts (Figure S1A). Thus, loss of AMPK α 1 activity in myeloid cells exacerbated lung tissue injury and skewed the balance of inflammatory leukocytes that entered the lung at baseline and following hookworm infection.

Type 2 immunity requires AMPK α 1 expression in myeloid APCs

AMPK deficiency has been shown to increase antigen-specific T_H1/T_H17 responses (9, 15, 16). Consistent with these reports, we found that helminth antigen-specific recall and T cell

mitogen responses were marked by highly elevated IFN- γ production in CD11cAMPK mice compared to WT when assessed at 9 dpi (Figure S1B). However, it has not been investigated whether AMPK serves as a driver of infection-induced Type 2 responses and because Type 2 cytokine production and M2 macrophage development has been proposed to drive tissue repair, we asked whether the CD11cAMPK strain had any defects in the production of canonical Type 2 cytokines and/or M2-associated molecules.

N.b. infection-induced release of Ym-1 (Chitinase-3 like 3) in BAL fluid (Figure 4A) and lung mRNA transcript levels for *Retnla* (Figure 4B) were significantly reduced in CD11cAMPK vs. the WT strain. Antigen-induced IL-13 production from whole splenocyte cultures was also significantly reduced in CD11cAMPK compared to WT (Figure 4C). Lung *Ii4* and *Cc117* mRNA transcripts were significantly reduced in CD11cAMPK mice compared to WT at 9 dpi (Figure D and E).

Next, we asked whether the CD11cAMPK strain had any defect in the accumulation of ILC2, a subset of cytokine-secreting innate lymphoid cells that promote the development of host-protective Type 2 immunity (17–19). Identification of ILC2 (defined as lineage negative CD45⁺IL-7R⁺Thy1.2⁺IL-17R β ⁺GATA3⁺) in whole lung tissue digests prepared from naïve (Figure 5A) and infected (Figure 5B) WT and CD11cAMPK strains revealed that CD11cAMPK mice had a significant defect in lung ILC2 expansion by day 3 (Figure 5C) whereas there were no differences between groups at baseline. Defective ILC2 expansion was corroborated by fewer *Areg* lung tissue mRNA transcripts, an EGF family cytokine (20) (Figure 5D). Double-immunofluorescence staining for YM-1 and CRTH2 (GPR44) on hookworm damaged lung tissue was used to determine whether the reduced numbers of ILC2 correlated with any alteration in the potential association between M2 and ILC2 *in situ*. Consistent with this hypothesis, data indicated that while many foci of YM-1/CRTH2 clusters were observed in WT mice, these interactions were less apparent within lung tissues of CD11cAMPK mice and their respective naïve controls (Figure S2A-D).

Next, parasitological analyses were conducted in order to assess the functional impact of the defective Type 2 immune responses on host protection against hookworm infection. Evaluation of CD11cAMPK and WT mice at 9 dpi revealed that CD11cAMPK mice had significantly higher hookworm egg and adult intestinal worm burdens compared to WT controls (Figure 5E and F). Given that CD4⁺ T cells displayed abnormally elevated AMPK levels in CD11cAMPK mice and that host immunity is CD4-dependent (21), we asked whether this T cell subset could be partially responsible for the impaired host-protective phenotype of the CD11cAMPK strain. Data show that RAG1^{-/-} mice passively transferred with CD4⁺ T cells purified from WT or CD11cAMPK strains and infected with *N.b.* showed an equivalent ability to reduce worm and egg burdens (Figure S3A and B, respectively) and to promote a rebound in pulmonary function (Figure S3C) as compared to non-transferred infected RAG1^{-/-} mice. Thus, defective M2 and ILC2-associated responses in CD11cAMPK mice were likely due to myeloid-intrinsic defects in AMPK activation following hookworm infection.

AMPK α 1 suppresses IL-12-dependent tissue injury and drives M2 polarization following hookworm infection

Immunity against *N. b.* is propelled by IL-4R α -dependent Type 2 immunity but is strongly suppressed by IL-12p40 (22). We reasoned that CD11cAMPK mice would show defaulted IL-12p40-associated inflammation. To investigate, magnetically sorted infected lung tissue CD11c⁺ cell mRNA transcripts were analyzed for IL-12/23p40 expression levels. Compared to WT animals, infected CD11cAMPK mice expressed 3-fold greater levels of *Il12b* cytokine transcript (Figure 6A) indicating an intrinsic defect due to AMPK deficiency. α -IL-12/23p40 neutralizing antibody (C17.8) was used to assess whether Type 2 immunity could be restored by neutralization of IL-12/23p40-associated inflammatory responses. Compared to isotype-matched control mAb (GL117), anti-IL-12/23p40 antibody administration increased the percentage of IL-13 cytokine-secreting splenic CD4⁺CD62L^{lo}CD44^{Hi} cells (Figure 6B, C). α -IL-12/23p40 antibody administration also significantly increased lung *Areg* expression (Figure 6D) and reversed the histological features of hookworm-induced lung injury (Figure 6E-H). Lastly, IL-12/23p40 neutralization increased the % SpO₂ in infected CD11cAMPK mice compared to those treated with GL117 control (Figure 6I). These findings demonstrated that myeloid-specific deletion of AMPK led to an IL-12-dependent suppression of IL-13-producing CD4⁺ T cells and ILC2 expansion.

Discussion

While it is well-established that metabolic status regulates tissue homeostasis at the organ level, it is only recently becoming recognized that metabolic enzymes can direct leukocyte function in a cell lineage-specific manner (15, 23–26). Our work demonstrates that AMPK promotes M2 development and restrains myeloid cell-driven IL-12 responses during infectious tissue injury, which has a vitally important role in promoting functional organ recovery following hookworm infection. AMPK deletion in alveolar macrophages and cDC reduced production of canonical M2 molecules, T_H2 cytokine production, and ILC2 expansion. Curiously, this phenotype was marked by reduced *Ccl17* production and fewer interactions between M2 and ILC2, which may imply a regulatory role for myeloid AMPK in producing chemokines required for ILC2 recruitment and/or expansion. Moreover, CD11c specific AMPK deficiency led to increased production of IL-12/23 p40, a T_H1/T_H17-inducing cytokine, which in turn, limited IL-13 production from CD4⁺ T cells and reduced ILC2-associated gene expression. Taken together, these data support the emerging concept that myeloid cells can regulate ILC2 and that mechanistically, myeloid cells utilize AMPK to promote Type 2 responses that are essential for parasite clearance and tissue repair following hookworm infection.

Following skin penetration, the lung is the first major organ system damaged by parasitic worms, which in some cases, leads to acute respiratory distress (27). *N.b.* rapidly migrates into the distal lung compartment within hours of infection where larvae destroy normal alveolar structure (10). AMPK α activity was up-regulated within 3 days, corresponding to peak hemorrhagic injury that precedes Type 2 cytokine production (14). While worm infection did not increase pAMPK MFI levels in alveolar macrophages on a per cell basis,

increased myeloid cell accumulation most likely contributed to increased AMPK levels in tissues. However, CD11c-mediated deletion led to an increase in AMPK levels, most likely because pAMPK levels were highly induced within CD4⁺ and CD8⁺ T cells by day 9, consistent with increasing energy demands during effector T cell development (28). Nonetheless, loss of AMPK α within alveolar macrophages and cDC abrogated the spontaneous rebound in lung function observed between 7-9 dpi with *N.b.* (13). As compared to WT controls, % SpO₂ levels were lower in CD11cAMPK mice by day 3. It is unlikely that the differences in % SpO₂ levels between strains were due solely to inflammatory leukocyte infiltration, because peak Type 2 inflammation and eosinophilia normally occur at day 9, when % SpO₂ levels are no different from baseline. Instead, % SpO₂ differences were likely due to defects in macrophage-dependent repair of pulmonary gas exchange. Histological comparison of hookworm-injured lungs revealed that CD11cAMPK mice had large distended alveoli, in contrast to WT lung pathology. However, it remains unclear whether macrophages can promote epithelial repair or only suppress cytokine release associated with the M1 pathway. The protective efficacy of α -IL-12/23p40 treatment suggests the latter and evidence that IFN- γ , a canonical Type 1 cytokine, can block Type 2 effector lymphocytes such as ILC2 (29), suggests that a predominate M1 cell response *in situ* may impair innate Type 2 responses.

The M2-associated molecules, Ym-1 and Relm- α , were produced in an AMPK α 1 dependent manner. However, it remains unclear whether AMPK also controls specific expression of molecules such as PD-L2 and Aldha1/2, which can distinguish between M2 cells derived from different sources (30). AMPK may directly favor M2 development through regulation of PPAR γ co-activators 1 α and β (PGC1 α/β), which are induced by IL-4/13 and support metabolic reprogramming associated with M2 polarization (31). Perhaps AMPK may function downstream of IL-4 to promote *Arg1* transcription, but this remains unknown. Whether there are discrete mediators released from M2 cells that promote tissue regeneration remains unknown and is the topic of future study (6, 32–35). Thus, while M2 cells may have secreted epithelial regenerative molecules, these factors have not been identified. Future work is needed to discern whether M2 cells derived from different sources or whether other macrophage phenotypes such as IL-10 or TGF- β -secreting cells or even N2 cells can elaborate selective mediators of epithelial cell regeneration.

Even though pharmacological activation of AMPK suppresses LPS-induced acute lung injury (36), the explanations for these effects were previously lacking. Our data are consistent with evidence that myeloid-specific AMPK drives IL-10/STAT-3 and PI3K/Akt/mTORC1-mediated suppression of pro-inflammatory cytokine production and CD40 expression (9, 15, 37). We demonstrate that neutralization of IL-12/23p40 (essential subunit for IL-12p70 and IL-23) partially reversed susceptibility of CD11cAMPK mice to severe lung injury and impaired respiratory function. This is consistent with evidence that IL-12 administration promotes susceptibility to *N.b.*(22) Lack of myeloid-derived AMPK α 1 also impaired infection-induced ILC2 expansion and lung *Areg* expression, which was reversed by IL-12/23p40 neutralization suggesting that myeloid cells can regulate ILC expansion due to the cytokines they produce. Indeed, defective *Cc117* expression and defective ILC2 responses are similar to a recent report in the context of allergic lung inflammation, where a coordinately regulated mechanism among T_H2, ILC2, and M2 drives the memory Type 2

response (38). Our demonstration that M2 and ILC2 are intimately associated in hookworm-damaged lungs is consistent with the view that these cells may modulate each other's activity. Indeed, increased IL-12 in parasitized CD11cAMPK mice accompanied by defective ILC2 responses is consistent with data showing that Type 1 inflammatory responses dominated by IFN- γ blocks ILC2 function (39). It will be important to determine whether myeloid derived IL-12/23p40 directly antagonizes ILC2 expansion, as *Areg* expression levels increased following anti-IL-12/23 p40 mAb administration. Similarly, CD4⁺T cell derived-IL-13 was restored upon IL-12/23p40 neutralization in CD11cAMPK mice. Thus, we extend findings that cDC depletion impairs T_H2 development (4) by revealing AMPK as an intrinsic determinant shaping the ability of myeloid APCs to promote Type 2 immunity.

Macrophages in the pulmonary compartment have dynamic roles in homeostasis, defense and repair, perhaps due to their unique lipid-rich environment (40). Indeed, lipolysis drives M2 polarization, a function that may occur through AMPK-dependent oxidative phosphorylation (25). Inclusive with studies demonstrating that IL-4 cytokine promotes Type 2 responses including proliferation and activation of Type 2 macrophages during *L. sigmodontis* infection (41), we propose that myeloid-derived AMPK contributes to the IL-4 driven pathway that promotes M2 polarization in the context of hookworm infection and lung injury

Supplementary Material

Refer to Web version on PubMed Central for supplementary material.

Acknowledgements

We thank Dr. Jill Suttles for critical reading of this manuscript and members of the Herbert lab for their technical support.

The National Institute of Health (NIH) Grants RO1-A1095289 and RO1-GM83204, Burrough's Wellcome Fund Award CA-0062619 (DRH) and an NIH Immunology T32 Research Training Grant and Diversity Supplement Award (WN) supported this work.

References

1. Xiao B, Sanders MJ, Underwood E, Heath R, Mayer FV, Carmena D, Jing C, Walker PA, Eccleston JF, Haire LF, Saiu P, Howell SA, Aasland R, Martin SR, Carling D, Gamblin SJ. Structure of mammalian AMPK and its regulation by ADP. *Nature*. 2011; 472:230–233. [PubMed: 21399626]
2. Towler MC, Hardie DG. AMP-activated protein kinase in metabolic control and insulin signaling. *Circ Res*. 2007; 100:328–341. [PubMed: 17307971]
3. Jäger S, Handschin C, St-Pierre J, Spiegelman BM. AMP-activated protein kinase (AMPK) action in skeletal muscle via direct phosphorylation of PGC-1 α . *Proc Natl Acad Sci U S A*. 2007; 104:12017–12022. [PubMed: 17609368]
4. Phythian-Adams AT, Cook PC, Lundie RJ, Jones LH, Smith KA, Barr TA, Hochweller K, Anderton SM, Hämmerling GJ, Maizels RM, MacDonald AS. CD11c depletion severely disrupts Th2 induction and development in vivo. *J Exp Med*. 2010; 207:2089–2096. [PubMed: 20819926]
5. Hotez PJ, Brindley PJ, Bethony JM, King CH, Pearce EJ, Jacobson J. Helminth infections: the great neglected tropical diseases. *J Clin Invest*. 2008; 118:1311–1321. [PubMed: 18382743]

6. Van Dyken SJ, Locksley RM. Interleukin-4- and interleukin-13-mediated alternatively activated macrophages: roles in homeostasis and disease. *Annu Rev Immunol.* 2013; 31:317–343. [PubMed: 23298208]
7. Mounier R, Théret M, Arnold L, Cuvelier S, Bultot L, Göransson O, Sanz N, Ferry A, Sakamoto K, Foretz M, Viollet B, Chazaud B. AMPK α 1 regulates macrophage skewing at the time of resolution of inflammation during skeletal muscle regeneration. *Cell Metab.* 2013; 18:251–264. [PubMed: 23931756]
8. Meares GP, Qin H, Liu Y, Holdbrooks AT, Benveniste EN. AMP-activated protein kinase restricts IFN- γ signaling. *J Immunol.* 2013; 190:372–380. [PubMed: 23180823]
9. Sag D, Carling D, Stout RD, Suttles J. Adenosine 5'-monophosphate-activated protein kinase promotes macrophage polarization to an anti-inflammatory functional phenotype. *J Immunol.* 2008; 181:8633–8641. [PubMed: 19050283]
10. Craig JM, Scott AL. Helminths in the lungs. *Parasite Immunol.* 2014; 36:463–474. [PubMed: 25201409]
11. Herbert DR, Yang JQ, Hogan SP, Groschwitz K, Khodoun M, Munitz A, Orekov T, Perkins C, Wang Q, Brombacher F, Urban JF, Rothenberg ME, Finkelman FD. Intestinal epithelial cell secretion of RELM-beta protects against gastrointestinal worm infection. *J Exp Med.* 2009; 206:2947–2957. [PubMed: 19995957]
12. Hung LY, Lewkowich IP, Dawson LA, Downey J, Yang Y, Smith DE, Herbert DR. IL-33 drives biphasic IL-13 production for noncanonical Type 2 immunity against hookworms. *Proc Natl Acad Sci U S A.* 2013; 110:282–287. [PubMed: 23248269]
13. Wills-Karp M, Rani R, Dienger K, Lewkowich I, Fox JG, Perkins C, Lewis L, Finkelman FD, Smith DE, Bryce PJ, Kurt-Jones EA, Wang TC, Sivaprasad U, Hershey GK, Herbert DR. Trefoil factor 2 rapidly induces interleukin 33 to promote type 2 immunity during allergic asthma and hookworm infection. *J Exp Med.* 2012; 209:607–622. [PubMed: 22329990]
14. Chen F, Liu Z, Wu W, Rozo C, Bowdridge S, Millman A, Van Rooijen N, Urban JF, Wynn TA, Gause WC. An essential role for TH2-type responses in limiting acute tissue damage during experimental helminth infection. *Nat Med.* 2012; 18:260–266. [PubMed: 22245779]
15. Carroll KC, Viollet B, Suttles J. AMPK α 1 deficiency amplifies proinflammatory myeloid APC activity and CD40 signaling. *J Leukoc Biol.* 2013; 94:1113–1121. [PubMed: 23883517]
16. Carroll, KC.; Viollet, B.; Suttles, J. 2013.
17. Barlow JL, Flynn RJ, Ballantyne SJ, McKenzie AN. Reciprocal expression of IL-25 and IL-17A is important for allergic airways hyperreactivity. *Clin Exp Allergy.* 2011; 41:1447–1455. [PubMed: 21722219]
18. Neill DR, McKenzie AN. Nuocytes and beyond: new insights into helminth expulsion. *Trends Parasitol.* 2011; 27:214–221. [PubMed: 21292555]
19. Neill DR, Wong SH, Bellosi A, Flynn RJ, Daly M, Langford TK, Bucks C, Kane CM, Fallon PG, Pannell R, Jolin HE, McKenzie AN. Nuocytes represent a new innate effector leukocyte that mediates type-2 immunity. *Nature.* 2010; 464:1367–1370. [PubMed: 20200518]
20. Monticelli LA, Sonnenberg GF, Abt MC, Alenghat T, Ziegler CG, Doering TA, Angelosanto JM, Laidlaw BJ, Yang CY, Sathaliyawala T, Kubota M, Turner D, Diamond JM, Goldrath AW, Farber DL, Collman RG, Wherry EJ, Artis D. Innate lymphoid cells promote lung-tissue homeostasis after infection with influenza virus. *Nat Immunol.* 2011; 12:1045–1054. [PubMed: 21946417]
21. Finkelman FD, Shea-Donohue T, Goldhill J, Sullivan CA, Morris SC, Madden KB, Gause WC, Urban JF. Cytokine regulation of host defense against parasitic gastrointestinal nematodes: lessons from studies with rodent models. *Annu Rev Immunol.* 1997; 15:505–533. [PubMed: 9143698]
22. Finkelman FD, Madden KB, Cheever AW, Katona IM, Morris SC, Gately MK, Hubbard BR, Gause WC, Urban JF. Effects of interleukin 12 on immune responses and host protection in mice infected with intestinal nematode parasites. *J Exp Med.* 1994; 179:1563–1572. [PubMed: 7909327]
23. Pearce EL, Poffenberger MC, Chang CH, Jones RG. Fueling immunity: insights into metabolism and lymphocyte function. *Science.* 2013; 342:1242454. [PubMed: 24115444]
24. Pearce EL, Pearce EJ. Metabolic pathways in immune cell activation and quiescence. *Immunity.* 2013; 38:633–643. [PubMed: 23601682]

25. Huang SC, Everts B, Ivanova Y, O'Sullivan D, Nascimento M, Smith AM, Beatty W, Love-Gregory L, Lam WY, O'Neill CM, Yan C, Du H, Abumrad NA, Urban JF, Artyomov MN, Pearce EL, Pearce EJ. Cell-intrinsic lysosomal lipolysis is essential for alternative activation of macrophages. *Nat Immunol.* 2014; 15:846–855. [PubMed: 25086775]
26. O'Sullivan D, van der Windt GJ, Huang SC, Curtis JD, Chang CH, Buck MD, Qiu J, Smith AM, Lam WY, DiPlato LM, Hsu FF, Birnbaum MJ, Pearce EJ, Pearce EL. Memory CD8(+) T cells use cell-intrinsic lipolysis to support the metabolic programming necessary for development. *Immunity.* 2014; 41:75–88. [PubMed: 25001241]
27. Phills JA, Harrold AJ, Whiteman GV, Perelmutter L. Pulmonary infiltrates, asthma and eosinophilia due to *Ascaris suum* infestation in man. *N Engl J Med.* 1972; 286:965–970. [PubMed: 5062734]
28. Blagih J, Coulombe F, Vincent EE, Dupuy F, Galicia-Vázquez G, Yurchenko E, Raissi TC, van der Windt GJ, Viollet B, Pearce EL, Pelletier J, Piccirillo CA, Krawczyk CM, Divangahi M, Jones RG. The energy sensor AMPK regulates T cell metabolic adaptation and effector responses in vivo. *Immunity.* 2015; 42:41–54. [PubMed: 25607458]
29. Molofsky AB, Van Gool F, Liang HE, Van Dyken SJ, Nussbaum JC, Lee J, Bluestone JA, Locksley RM. Interleukin-33 and Interferon- γ Counter-Regulate Group 2 Innate Lymphoid Cell Activation during Immune Perturbation. *Immunity.* 2015; 43:161–174. [PubMed: 26092469]
30. Gundra UM, Girgis NM, Ruckerl D, Jenkins S, Ward LN, Kurtz ZD, Wiens KE, Tang MS, Basu-Roy U, Mansukhani A, Allen JE, Loke P. Alternatively activated macrophages derived from monocytes and tissue macrophages are phenotypically and functionally distinct. *Blood.* 2014
31. Vats D, Mukundan L, Odegaard JI, Zhang L, Smith KL, Morel CR, Wagner RA, Greaves DR, Murray PJ, Chawla A. Oxidative metabolism and PGC-1 β attenuate macrophage-mediated inflammation. *Cell Metab.* 2006; 4:13–24. [PubMed: 16814729]
32. Jang JC, Nair MG. Alternatively Activated Macrophages Revisited: New Insights into the Regulation of Immunity, Inflammation and Metabolic Function following Parasite Infection. *Curr Immunol Rev.* 2013; 9:147–156. [PubMed: 24772059]
33. Osborne LC, Monticelli LA, Nice TJ, Sutherland TE, Siracusa MC, Hepworth MR, Tomov VT, Kobuley D, Tran SV, Bittinger K, Bailey AG, Laughlin AL, Boucher JL, Wherry EJ, Bushman FD, Allen JE, Virgin HW, Artis D. Coinfection. Virus-helminth coinfection reveals a microbiota-independent mechanism of immunomodulation. *Science.* 2014; 345:578–582. [PubMed: 25082704]
34. Ferrante CJ, Leibovich SJ. Regulation of Macrophage Polarization and Wound Healing. *Adv Wound Care (New Rochelle).* 2012; 1:10–16. [PubMed: 24527272]
35. Vannella KM, Barron L, Borthwick LA, Kindrachuk KN, Narasimhan PB, Hart KM, Thompson RW, White S, Cheever AW, Ramalingam TR, Wynn TA. Incomplete deletion of IL-4R α by LysM(Cre) reveals distinct subsets of M2 macrophages controlling inflammation and fibrosis in chronic schistosomiasis. *PLoS Pathog.* 2014; 10:e1004372. [PubMed: 25211233]
36. Zhao X, Zmijewski JW, Lorne E, Liu G, Park YJ, Tsuruta Y, Abraham E. Activation of AMPK attenuates neutrophil proinflammatory activity and decreases the severity of acute lung injury. *Am J Physiol Lung Cell Mol Physiol.* 2008; 295:L497–L504. [PubMed: 18586954]
37. Zhu YP, Brown JR, Sag D, Zhang L, Suttles J. Adenosine 5'-monophosphate-activated protein kinase regulates IL-10-mediated anti-inflammatory signaling pathways in macrophages. *J Immunol.* 2015; 194:584–594. [PubMed: 25512602]
38. Halim TY, Hwang YY, Scanlon ST, Zaghouni H, Garbi N, Fallon PG, McKenzie AN. Group 2 innate lymphoid cells license dendritic cells to potentiate memory TH2 cell responses. *Nat Immunol.* 2016; 17:57–64. [PubMed: 26523868]
39. Kudo F, Ikutani M, Seki Y, Otsubo T, Kawamura YI, Dohi T, Oshima K, Hattori M, Nakae S, Takatsu K, Takaki S. Interferon- γ Constrains Cytokine Production of Group 2 Innate Lymphoid Cells. *Immunology.* 2015
40. Whitsett JA, Alenghat T. Respiratory epithelial cells orchestrate pulmonary innate immunity. *Nat Immunol.* 2014; 16:27–35. [PubMed: 25521682]

41. Jenkins SJ, Ruckerl D, Cook PC, Jones LH, Finkelman FD, van Rooijen N, MacDonald AS, Allen JE. Local macrophage proliferation, rather than recruitment from the blood, is a signature of TH2 inflammation. *Science*. 2011; 332:1284–1288. [PubMed: 21566158]

Author Manuscript

Author Manuscript

Author Manuscript

Author Manuscript

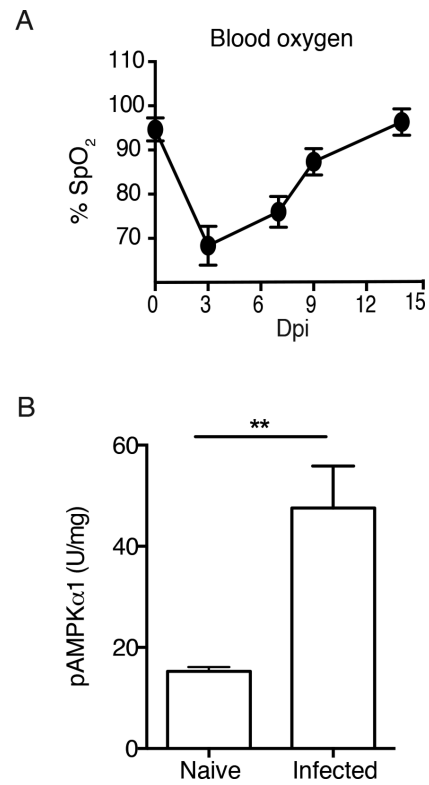


Fig. 1. Hookworm infection increases lung injury and AMPK α activation

A) Percentage SpO₂ of *N.b.*-infected WT mice. B) Data show pAMPK α levels in whole lung tissue lysates from WT C57BL/6 mice left un-treated (naïve) or at 3 days post-infection (Dpi) with 750 *N.b.* L₃. Data represents 2 independent experiments (n=3/group), SEM. **p<0.01

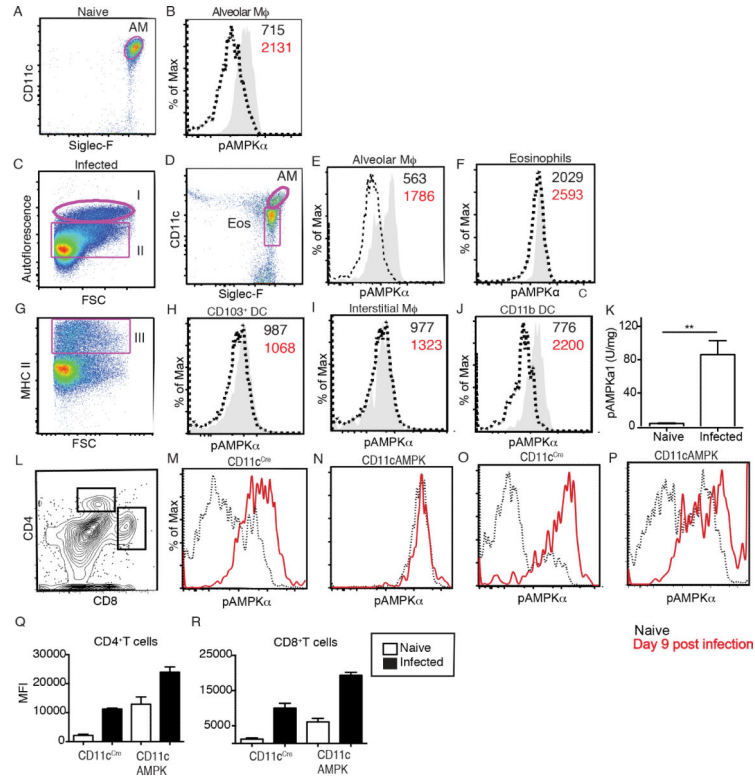


Fig. 2. Characterization of the AMPK activation status in CD11cAMPK mouse-derived pulmonary leukocytes during hookworm infection

A-J) AMPK α -specific intracellular staining to compare CD11cAMPK (dotted line) and CD11c^{Cre} (gray histogram) for median fluorescence intensity expression levels in A, B) alveolar macrophages of naïve mice. C-E) MFI levels for AMPK α ICS at 9 dpi in autofluorescent alveolar macrophages and F) non-autofluorescent eosinophils (n=4/group). G-J) MFI expression levels in MHC-II^{POS}, H) CD103⁺ DC, I) interstitial macrophages (M ϕ), and J) CD11b DC (n=4). K) Data show pAMPK α levels in whole lung tissue lysates from WT C57BL/6 mice left un-treated (naïve) or at 3 dpi with 750 *N.b.* L₃ (n=3/group). L) Contour plot shows gating strategy for splenic CD4⁺ and CD8⁺ T cell gating. M-P) Representative MFI histograms from two independent experiments (n=4/group) show M, N) CD4⁺ T cells and O, P) CD8⁺ T cells from naïve (dotted line) vs. 9 day *N.b.*-infected (red line) CD11c^{Cre} and CD11cAMPK mice. Mean \pm SEM of MFI levels of AMPK α staining in gated Q) CD4⁺ T cells and R) CD8⁺ T cells from 4 mice/group. All data represents 2-3 independent experiments. *p<0.05, **p<0.01, ***p<0.001

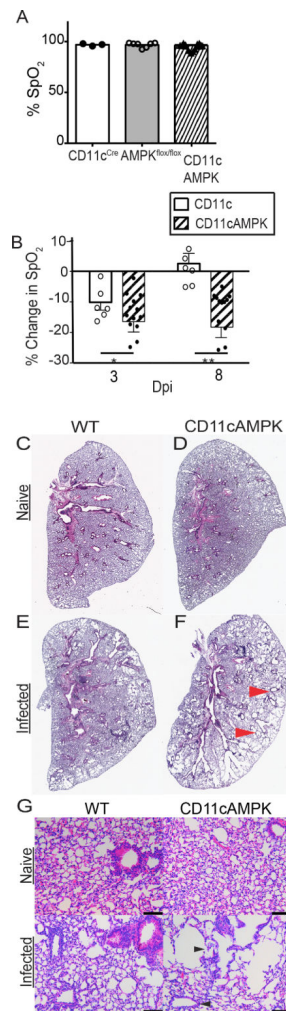


Fig 3. Deletion of AMPK α in myeloid cells exacerbates lung injury

A) Raw % SpO₂ of naïve WT (CD11c^{Cre} and AMPK^{flox/flox}) and CD11cAMPK mice. N=3-10. Data is representative of 3 independent experiments. B) Change in % SpO₂ from baseline levels at 3 and 8 dpi; n=6-10. C-D) H&E-stained left lobe of naïve or (E,F) 9 day infected lung tissue. Red arrows indicate areas of tissue injury. G) 20x magnification of H&E-stained histological cross-sections of the left lobe from naïve or 9 day infected WT and CD11cAMPK mice. Black arrows indicate areas of tissue injury and distended alveoli. Bar indicates 100 μm. Data represent 2-4 experiments SEM. *p<0.05, **p<0.01, ***p<0.001

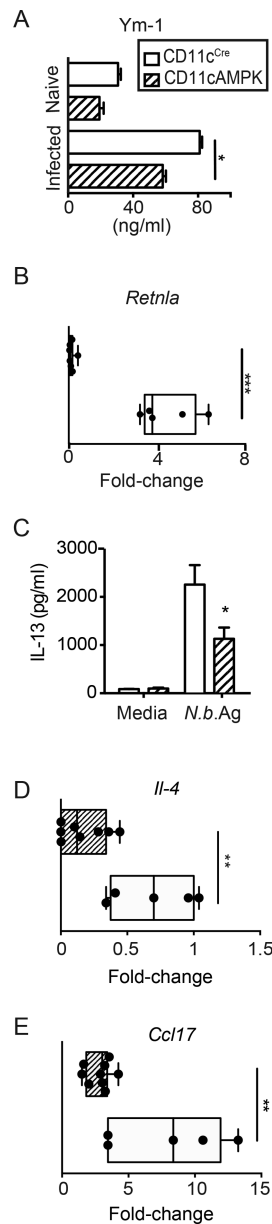


Fig. 4. Myeloid pAMPK α 1 deficiency impairs M2 responses and hookworm-induced IL-13 production

Comparison of naïve and 9 day infected CD11c^{Cre} and CD11cAMPK mice for A) Ym-1 protein levels in BAL fluid, B) lung mRNA transcript levels for *Retnla*. Fold-expression of infected over respective naïve controls. C) IL-13 levels in splenocyte culture supernatants following stimulation with crude *N.b.* antigen extract (*N.b.* Ag) or left un-treated (control). D) Fold-change of lung *il4* and E) *Ccl17* mRNA transcript levels. Fold-expression of infected over respective naïve controls. Data show mean \pm SEM and represent 3 independent experiments 3-8 mice/group. *p<0.05, **p<0.01, ***p<0.001

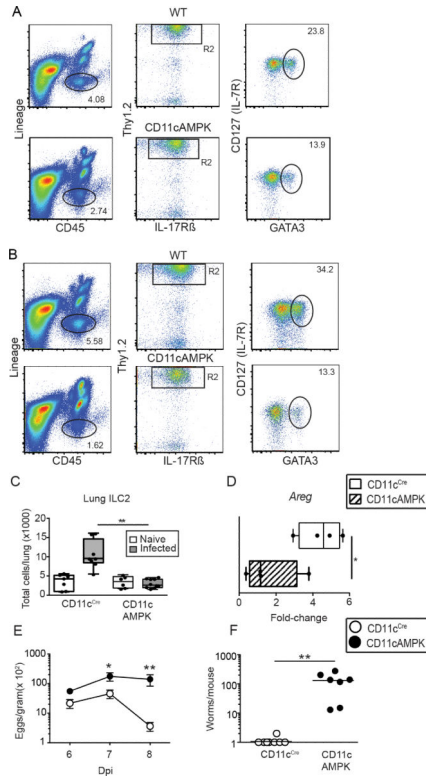


Fig. 5. Myeloid pAMPKα1 deficiency impairs hookworm-induced ILC2 expansion

A) Flow cytometry dot plot shows the percentage of lung ILC2 within lung tissue digests from CD11c^{Cre} (Top) and CD11cAMPK (bottom) naïve and B) infected mice 3 Dpi. Percentage of lung population indicated on plot. C) Total ILC2 cell number per lung of naïve and infected mice. D) Lung mRNA transcript levels for *Areg*. Fold-expression of infected over respective naïve controls. E) Fecal egg counts per gram of tissue 6, 7, and 8 dpi and F) number of adult intestinal worms 9 dpi with *N.b*. Data show mean± SEM and represent 3 independent experiments 3-5 mice/group. *p<0.05, **p<0.01, ***p<0.001

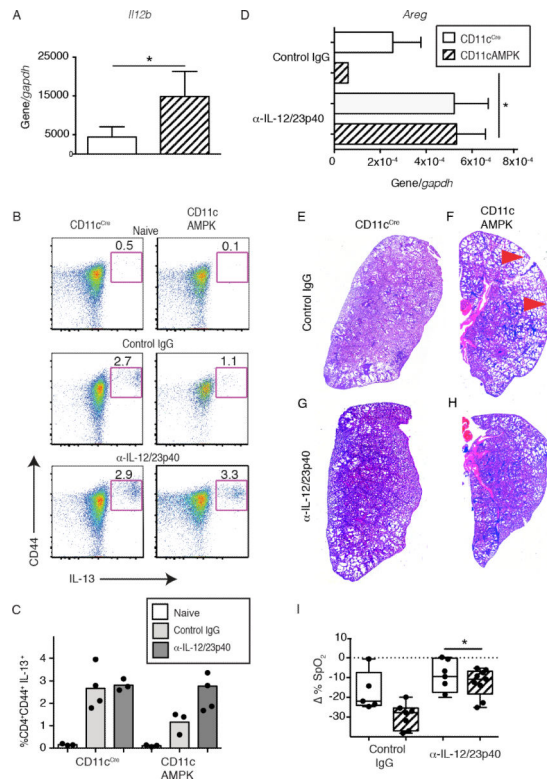


Fig. 6. Neutralization of IL-12/23 p40 in CD11cAMPK mice restores Type 2 responses and lung repair

A) Comparison of whole tissue mRNA transcript levels for *Il12b* from sorted pulmonary CD11c⁺ cells between CD11c^{Cre} and CD11cAMPK mice at 9 dpi with *N.b.* B) Representative dot plots showing the percentage of CD4⁺CD62^{L0}CD44^{Hi}IL-13⁺ cells within the spleen of naïve (top) or at 9 dpi following IgG2a isotype mAb (middle), or anti-IL-12/23p40 mAb-treatment (bottom) mice. C) Dot plot showing the percentage of CD4⁺CD62^{L0}CD44^{Hi}IL-13⁺ cells within the spleen of naïve (white), or at 9 Dpi following isotype mAb (gray), or anti-IL-12/23p40 mAb-treatment (charcoal) mice. D) *Areg* mRNA transcript of lung tissue from CD11c^{Cre} (solid) and CD11cAMPK (hatched) mice 9 dpi with *N. b.* L₃. Graph indicates relative expression over the *Gapdh* reference gene. H&E-stained cross-section of left lobe of lung (200x magnification) from G, H) isotype mAb or I, J) anti-IL-12/23p40 mAb-treatment. Red arrows indicate areas of lung injury. F) Change in % SpO₂ at 8 dpi following treatment with 3 doses of 1mg anti-IL-12/23p40 mAb or IgG2a isotype mAb. Data represent two independent experiments containing 3-5 mice per group. *p<0.05, **p<0.01